Title: Molecular basis for the maintenance of lipid asymmetry in the outer membrane of *Escherichia coli*

Authors: Jiang Yeow[a,b,1], Kang Wei Tan[a,1], Daniel A. Holdbrook[c,1], Zhi-Soon Chong[a], Jan K. Marzinek[c,d], Peter J. Bond[c,d,*], Shu-Sin Chng[a,e,*]

Affiliations:

[a]Department of Chemistry, National University of Singapore, Singapore 117543.

[b]National University of Singapore Graduate School for Integrative Sciences and Engineering (NGS), Singapore 117456.

[c]Bioinformatics Institute, Agency for Science, Technology, and Research (A*STAR), Singapore 138671.

[d]Department of Biological Sciences, National University of Singapore, Singapore 117543.

[e]Singapore Center for Environmental Life Sciences Engineering, National University of Singapore (SCELSE-NUS), Singapore 117456.

[1]These authors contributed equally to this work.

*To whom correspondence should be addressed. E-mail: chmchngs@nus.edu.sg, peterjb@bii.a-star.edu.sg

Author contributions: J.Y., K.W.T., D.A.H., P.J.B. and S.-S.C designed research; J.Y., K.W.T., Z.-S.C. performed all wet lab experiments described in this work; D.A.H. and J.K.M. performed all MD simulations; J.Y., K.W.T., D.A.H., P.J.B. and S.-S.C. analyzed and discussed data; J.Y., K.W.T., and S.-S.C. wrote the paper.

The authors declare no conflict of interest.

Abstract

A distinctive feature of the Gram-negative bacterial cell envelope is the presence of an asymmetric outer membrane (OM), where lipopolysaccharides (LPS) and phospholipids (PLs) reside in the outer and inner leaflets, respectively. This unique lipid asymmetry renders the OM impermeable to external insults, thus allowing survival of bacteria in harsh environments. In *Escherichia coli*, the OmpC-Mla system is responsible for maintenance of OM lipid asymmetry. Osmoporin OmpC and the OM lipoprotein MlaA form a complex proposed to remove PLs from the outer leaflet of the OM. How this complex is organized in the OM to perform this function is not known. In this report, we define the molecular architecture of the OmpC-MlaA complex to gain insights into its function in PL transport. We show that MlaA sits entirely within the OM lipid bilayer, and interacts with the OmpC trimer at its dimeric interfaces. Molecular dynamics simulations reveal a membrane-spanning hydrophilic channel within MlaA, suggesting a path for PL translocation across the OM. We demonstrate that a hydrophobic hairpin loop adjacent to this putative channel is critical for modulating the activity of MlaA; restricting flexibility of this structure significantly perturbs the function of the complex. Finally, we establish that OmpC plays an active role in maintaining OM lipid asymmetry together with MlaA. Our work provides a glimpse into the molecular mechanism of how the OmpC-MlaA complex may extract PLs from the outer leaflet of the OM, and highlights key features that could be exploited in the development of future antimicrobial drugs.

Keywords

lipid asymmetry, phospholipid transport, photoactivable crosslinking, molecular modelling, PagP-mediated acylation

Introduction

The outer membrane (OM) of Gram-negative bacteria is an extremely asymmetric bilayer, comprising lipopolysaccharides (LPS) in the outer leaflet and phospholipids (PLs) in the inner leaflet (1, 2). LPS molecules pack tightly together in the presence of divalent cations to form an outer layer with markedly reduced fluidity and permeability (3). Thus, the OM serves as an effective barrier against toxic compounds including detergents and antibiotics. This function is fully dependent on the establishment and maintenance of lipid asymmetry; cells generally become more sensitive to external insults when OM lipid asymmetry is disrupted, which is typically characterized by the accumulation of PLs in the outer leaflet (4, 5). The OM is also essential for viability.

The requisite lipid asymmetry of the OM is likely initially established by direct placement of LPS and PLs into the outer and inner leaflets, respectively. LPS assembly into the outer leaflet of the OM is mediated by the well-established Lpt (lipopolysaccharide transport) machinery (6), but proteins that transport and insert PLs into the inner leaflet have not been identified. For entropic reasons, there is a natural tendency for PLs to appear in the outer leaflet of the OM, although how they traverse the bilayer is unclear. This occurs more readily with perturbations in the OM, especially when assembly of other OM components is disrupted (4, 5, 7). Since loss of lipid asymmetry compromises the barrier function of the OM, several mechanisms exist to remove PLs aberrantly localized in the outer leaflet of the membrane: (i) the OM phospholipase OmpLA hydrolyzes both acyl chains from outer leaflet PLs (8), (ii) the OM acyltransferase PagP transfers an acyl chain from outer leaflet PLs to LPS (9) or phosphatidylglycerol (PG) (10), and (iii) the OmpC-Mla system, a putative PL trafficking pathway, removes outer leaflet PLs and shuttles them back to the inner membrane (IM) (11, 12).

The OmpC-Mla system comprises seven proteins located across the cell envelope. Removing any component results in PL accumulation in the outer leaflet of the OM, and therefore sensitivity to SDS/EDTA (11, 12). The OM lipoprotein MlaA forms a complex with osmoporin OmpC that likely extracts PLs from the outer leaflet of the OM (12). The periplasmic protein MlaC serves as a lipid chaperone and is proposed to transport lipids from the OmpC-MlaA complex to the IM (11, 13, 14). At the IM, MlaF and MlaE constitute an ATP-binding cassette (ABC) family transporter together with two auxiliary proteins, MlaD and

MlaB (14, 15); this complex presumably receives PLs from MlaC and inserts them into the membrane. MlaD has been shown to bind PLs, while MlaB is important for both assembly and activity of the transporter (15). Recently, the function of the OmpC-Mla system in retrograde (OM-to-IM) PL transport has been demonstrated in *E. coli* (7).

The molecular mechanism by which the OmpC-MlaA complex extracts PLs from the outer leaflet of the OM, presumably in an energy-independent manner, is an interesting problem. Aside from the LptDE machine, which assembles LPS on the surface (4, 5), the OmpC-MlaA complex is the only other system proposed to catalyze the translocation of lipids across the OM. OmpC is a classical trimeric porin that typically only allows passage of hydrophilic solutes across the OM (3, 16), while MlaA is believed to be anchored to the inner leaflet of the membrane; how the two proteins are organized in a complex for the translocation of amphipathic PLs is not known. In this paper, we establish that MlaA is in fact an integral membrane protein that forms a channel adjacent to OmpC trimers in the OM, likely allowing the passage of PLs. We first demonstrated that MlaA binds the OmpC trimer within the OM bilayer by mapping the interaction surfaces using in vivo crosslinking. Using a recently predicted structural model of MlaA (17), we obtained molecular views of the OmpC-MlaA complex by molecular dynamics (MD) simulations, and discovered a hydrophilic channel within OM-embedded MlaA. Combining charge mutations in this channel modulated MlaA activity, suggesting functional importance. Furthermore, mutations altering the flexibility of a hairpin loop that could interact with the hydrophilic channel led to predictable in vivo effects on MlaA function. Finally, we identified a key residue on OmpC found at the OmpC-MlaA interacting surface that is important for proper function of the complex. Our findings provide important mechanistic insights into how PLs may be translocated across the OM to ensure proper lipid asymmetry.

Results

The OmpC trimer contacts MlaA directly along its membrane-facing dimeric interfaces.

To develop a detailed architectural understanding of the OmpC-MlaA complex, we carried out in vivo photocrosslinking to map the intermolecular interactions within the complex. Guided by the crystal structure of OmpC trimers (18), we introduced the UV-crosslinking amino acid, *para*-benzoyl-L-

phenylalanine (*p*Bpa), at 49 positions in OmpC via amber suppression (19). Initial selection focused on residues that are either solvent-accessible (i.e. loop and lumen residues) or located near the membrane-water boundaries (i.e. aromatic girdle residues). Upon UV irradiation, a ~65 kDa crosslinked band that contains both OmpC (~37 kDa) and MlaA (~28 kDa) could be detected in cells expressing OmpC variants substituted with *p*Bpa at three positions (L50, Q83, or F267) (Fig. 1*A*). These residues are found on the periplasmic turns at the dimeric interfaces of the OmpC trimer (Fig. 1*C*), thus localizing possible binding sites for MlaA. We have previously proposed that OmpC may allow MlaA to traverse the bilayer and gain access to PLs that have accumulated in the outer leaflet of the OM (12). As none of the six selected residues in the OmpC lumen crosslinked to MlaA, we decided to probe for interactions between MlaA and the membrane-facing side walls of OmpC, specifically around the dimeric interfaces of the OmpC trimer. Remarkably, out of the additional 49 positions tested in this region, 10 residues allow photoactivated crosslinks between OmpC and MlaA when replaced with *p*Bpa (Fig. 1*B* and Fig. S1). In total, these 13 crosslinking residues clearly demarcate an extensive MlaA-interacting surface on OmpC (Fig. 1*C*). This explains why OmpC exhibits strong interactions, and can be co-purified with MlaA on an affinity column, as we have previously reported (12). One position, Y149, is located right at the membrane-water boundary exposed to the extracellular environment, suggesting that MlaA traverses the entire width of the OM. We conclude that MlaA binds along the dimeric interfaces of the OmpC trimer in the membrane.

Two specific regions on MlaA contact the membrane-facing dimeric interfaces of the OmpC trimer.

We sought to map in greater detail the OmpC-MlaA interacting surface in vitro. To do that, we first overexpressed and purified the OmpC-MlaA complex to homogeneity. We showed that this complex forms a single peak on size exclusion chromatography (SEC) (Fig. 2*A*). OmpC within this complex exhibits the characteristic heat-modifiable gel shift commonly observed for OM β-barrel proteins (20), consistent with the presence of the folded trimer. Multi-angle light scattering (MALS) analysis revealed that one copy of MlaA interacts with the OmpC trimer (Fig. S2), suggesting that only one of the three dimeric interfaces within the trimer is available for binding (Fig. 1*C*). We next performed protease digestion experiments to identify specific region(s) on MlaA that may interact stably with OmpC. OM β-barrel proteins such as

OmpC are known to be protease-resistant (21). Given that some parts of MlaA contact OmpC within the membrane, we expect these bound regions to also be protected from proteolytic degradation. Treatment of the purified OmpC-MlaA complex with trypsin results in almost complete degradation of MlaA, with the OmpC trimer remaining intact (Fig 2*A*). Following SEC, however, we found that an ~8 kDa peptide (presumably from MlaA) remains stably bound to the trimer. N-terminal sequencing and tandem mass spectrometry (MS) analyses revealed that this peptide corresponds to $MlaA_{D61\text{-}K124}$ (Figs. 2*A* and 2*C*, and Fig. S3). These results suggest that MlaA interacts strongly with OmpC in the membrane in part via this specific region.

To define how OmpC contacts the $MlaA_{D61\text{-}K124}$ peptide, we next attempted to overexpress and purify *p*Bpa-containing OmpC variants in complex with MlaA, and determine which of the previously identified 13 OmpC residues interacts with $MlaA_{D61\text{-}K124}$ in vitro. We sequentially performed UV crosslinking and trypsin digestion to potentially link $MlaA_{D61\text{-}K124}$ to specific residues on OmpC. This approach may also allow trapping of other potential interacting regions of MlaA, which might not have been stably retained on the wild-type complex after trypsin digestion. We successfully detected trypsin-resistant crosslinked products for seven $OmpC_{p\mathrm{Bpa}}$-MlaA complexes (Fig. 2*B*); these appeared slightly above OmpC between 37 to 50 kDa, indicating that peptides in the range of ~6-10 kDa are crosslinked to OmpC. N-terminal sequencing of six of the seven adducts showed the presence of OmpC, and an MlaA peptide beginning at residue D61 (Figs. 2*C* and 2*D*, and Fig. S3). Given the approximate sizes of the crosslinked adducts, we concluded that all these residues interact with $MlaA_{D61\text{-}K124}$. Interestingly, an additional peptide on MlaA starting at residue F133 was also found to crosslink at two (Y149 and L340) of these six positions on OmpC (Figs. 2*B–D*, and Fig. S3). These adducts can be detected by an α-MlaA antibody that recognizes an epitope within V182-Q195 on MlaA (Fig. 2*B*), suggesting that a peptide from F133 to at least R205 (next trypsin cleavage site) may be crosslinked (Fig. 2*C*). Thus, in addition to $MlaA_{D61\text{-}K124}$, our crosslinking strategy revealed a second point of contact ($MlaA_{F133\text{-}R205}$) between OmpC and MlaA.

There is no available molecular structure for MlaA; however, a structural model has been predicted based on residue-residue contacts inferred from coevolution analysis of metagenomic sequence data (17). Using a rigorously-validated quality score, this method of structure determination has generated reliable

models for 614 protein families with currently unknown structures. We experimentally validated the model for MlaA by replacing residue pairs far apart on the primary sequence with cysteines, and showed that only those that are highly co-evolved (and predicted to be residue-residue contacts) allow disulfide bond formation (Fig. S4). We therefore proceeded to use this MlaA model to understand the organization of the OmpC-MlaA complex. Interestingly, the positions of the two OmpC-contacting peptides on the MlaA model are spatially separated in a way consistent with the arrangement of the residues on OmpC that crosslink to each peptide (Fig. 2*D*). This not only reveals how MlaA may potentially be oriented and organized around the dimeric interface of the OmpC trimer, but also suggests that the entire MlaA molecule may reside in the membrane. In fact, the overall surface of MlaA, other than the putative periplasmic-facing region, is largely hydrophobic (Fig. S5). Furthermore, using all-atomistic MD simulations, we found that the structural fold of MlaA appears to be much more stable in a lipid bilayer than in an aqueous environment (Fig. S6). Consistent with this, we note that even without its N-terminal lipid anchor, MlaA is not a soluble protein, and can only be extracted and purified from the OM in the presence of detergent. Collectively, these observations lend strong support to the validity of the predicted MlaA structure.

Molecular models of the OmpC-MlaA complex suggests a path for PL translocation across the OM.

To obtain a physical picture of how OmpC interacts with MlaA within the complex, we used MD simulations to dock MlaA onto the OmpC trimer within a PL bilayer. Using a previously reported protocol (22), we first docked the MlaA model onto the OmpC trimer structure, both as rigid bodies. Interestingly, all initial docked structures contained MlaA binding at one dimeric interface of OmpC. Based on information derived from crosslinking, we selected the most consistent model for unrestrained refinement using all-atomistic simulations in a PL bilayer, where both OmpC and MlaA are allowed to relax. Three separate simulations were run until overall root-mean-square deviations (RMSD) stabilized; remarkably, the resulting models fulfilled all observed experimental crosslinking data. Using the RMSD data, we performed clustering on all three trajectories and identified four most populated conformations of the OmpC-MlaA complex (Fig. 3*A*, and Fig. S7). These conformational models all show MlaA sitting in the bilayer, tucked nicely into the dimeric interface of the OmpC trimer. Interestingly, three of these models also revealed the

presence of one outer leaflet PL molecule sandwiched in between OmpC and MlaA at the interacting surface (Fig. S8*A*), which may have implications for how the OmpC-MlaA complex access outer leaflet PLs (see Discussion). Evidently, the $MlaA_{D61-K124}$ peptide interacts extensively with OmpC in all the models (Fig. 3*A*, and Fig. S7), consistent with why this peptide remains stably-bound to OmpC after protease digestion (Fig. 2*A*). In contrast, only a small segment (F169-L173) of the $MlaA_{F133-R205}$ peptide makes contact with OmpC, and only in two of four conformational models (Fig. 3*A*, and Fig. S7), suggesting possible flexibility in this region. To validate the OmpC-MlaA models, we mutated several MlaA residues found at the OmpC-MlaA interface to *p*Bpa, and performed in vivo crosslinking experiments. We identified one position, L109, that allows strong photoactivatable crosslinking to OmpC when replaced with *p*Bpa (Fig. 3*B*). This residue lies within the $MlaA_{D61-K124}$ peptide, confirming that this region does in fact contact OmpC, as illustrated in the model (Fig. 3*C*).

One striking feature present in all the simulated OmpC-MlaA structures is a negatively-charged hydrophilic channel within MlaA that spans the lipid bilayer (Fig. 4*A*, and Fig. S9). Based on its function in removing PLs from the outer leaflet of the OM, we hypothesize that this channel may allow passage of charged headgroups as PLs translocate across the membrane. Interestingly, coarse-grained simulations of the OmpC-MlaA models in an OM bilayer showed outer leaflet PLs being attracted to the opening of the channel via their headgroups (Fig. S8*B*). To test this idea, we separately mutated 19 polar and (negatively) charged residues near or within the channel to alanine or arginine, and tested for MlaA function. However, all of these MlaA mutants are functional (Fig. 4*C*, and Fig. S10), indicating that single residue changes are not sufficient to perturb channel properties to affect PL transport. We noticed that four (D160, D161, D164, and D167) of the five negatively-charged channel residues are in close proximity on a single α-helix (Fig. 4*B*). To alter channel properties more drastically, we combined alanine or arginine mutations for the first three aspartates (*3D3A* or *3D3R*, respectively); interestingly, only the *3D3R* mutation disrupted function. Cells expressing only $MlaA_{3D3R}$ are highly sensitive to SDS/EDTA (Fig. 4*C*), likely due to accumulation of PLs in the outer leaflet of the OM (as judged by PagP-mediated acylation of LPS; Fig. 4*D*). In fact, this mutant exhibits OM defects that are more pronounced than the Δ*mlaA* strain (Fig. 4*C*), suggesting gain of function. Consistent with this idea, the *3D3R* mutation gives rise to the same defects in strains also

expressing the wild-type *mlaA* allele, revealing a dominant negative phenotype. We showed that $MlaA_{3D3R}$ is produced at levels comparable to wild-type MlaA on a plasmid (Fig. S11*A*), and is still able to interact strongly with OmpC (Fig. S11*B*). Taken together, these results suggest that the MlaA channel plays a functional role in PL transport.

Flexibility of a hairpin loop on MlaA distal to the OmpC-MlaA interface is required for function.

The gain-of-function/dominant negative phenotype of the $mlaA_{3D3R}$ mutant is similar to a previously reported *mlaA** (or $mlaA_{\Delta NF}$) mutant (Figs. 4*B* and 4*C*) (23), suggesting that these mutations may have similar effects on MlaA structure and/or function. Interestingly, the positions of these mutations on the OmpC-MlaA models flank a hydrophobic hairpin loop (G141-L158) within MlaA (Fig. 5*A*). Therefore, we hypothesized that the loop could play a functional role in MlaA, and that these mutations may affect interactions with this loop. To examine this possibility, we created three separate mutations at the hairpin structure and tested each variant for MlaA function. Two of these mutations, Y^{147}VQL→4A (*L1*) and F^{152}YGSF→5A (*L2*), are designed to disrupt interactions with other regions of the complex. The other mutation, P151A, removes a proline that may be critical for the hairpin turn structure. The N-terminus of the loop is connected to the rest of MlaA via an unstructured glycine-rich linker, which we reasoned may influence conformation of the entire hairpin structure. Thus, we constructed two additional mutants, G^{141}VGYG→A^{141}VAYA (*3G3A*) and G^{141}VGYG→P^{141}VPYP (*3G3P*), to reduce possible flexibility in this region. Remarkably, *L1*, *L2*, and *3G3P* mutations resulted in similar extents of SDS/EDTA sensitivity (Fig. 5*B*), as well as OM outer leaflet PL accumulation (Fig. 5*C*), when compared to the Δ*mlaA* mutation. Given that these mutations also do not affect MlaA levels or interaction with OmpC (Fig. S11), we conclude that they are loss-of-function mutations. The hairpin loop, along with its surrounding structures, forms an important functional region on MlaA.

Phenotypes observed for the loop rigidifying mutation (*3G3P*) and gain-of-function mutations (*3D3R* and *mlaA**) suggest that flexibility in the hairpin loop is critical for MlaA function. We hypothesize that the hairpin loop may exist in two distinct conformations. The *3D3R* or *mlaA** mutations could alter interactions with the loop, resulting in it adopting one conformation, and somehow giving rise to gain-of-

function/dominant negative phenotypes; in the case of *mlaA**, it was proposed that this mutation caused MlaA to be in a "leaky" or "open" state, and allowed PLs to flip out to the outer leaflet of the OM (23). In contrast, the *3G3P* mutation may lock the hairpin loop in a second conformation, where MlaA is in a "closed" state, thus abolishing function in PL transport. If these were true, we predict that rigidification of the hairpin loop with the *3G3P* mutation would be able to correct gain-of-function/dominant negative phenotypes observed in the *3D3R* and/or *mlaA** mutants. Indeed, the *3G3P/3D3R* and *3G3P/mlaA** combination mutants no longer exhibit gain-of-function/dominant negative phenotypes, but behave like the *3G3P* or null mutants (Fig. 5*D*). Again, these variants are expressed at comparable levels to the single mutants, and still interact with OmpC (Fig. S11). Taken together, these results indicate clear importance of dynamics in the hairpin loop in controlling the function of MlaA.

A specific residue in the dimeric interface of OmpC is important for its function in maintaining lipid asymmetry.

Given that MlaA sits in the membrane and provides a channel that putatively allows movement of PLs across the OM, it is not clear why it should bind at one of the dimeric interfaces of OmpC trimers, and what the exact role of OmpC may be. To understand the importance of OmpC-MlaA interaction, we attempted to engineer monomeric OmpC constructs that we predict would no longer interact with MlaA. We installed specific mutations (G19W and/or R92L) in OmpC that were found previously to disrupt the oligomerization state of its homolog OmpF (G19W and R100L correspondingly) in vitro (24) (Fig. 6*A*). Both the $OmpC_{G19W}$ and $OmpC_{R92L}$ single mutants can interact with MlaA, and still form trimers in vitro, albeit slightly destabilized compared to wild-type OmpC (Fig. S12). Combination of these mutations further weakens the OmpC trimer, with noticeable monomer population at physiological temperature. Intriguingly, both the double mutant and the R92L single mutant accumulated PLs in the outer leaflet of the OM (Fig. 6*B*), indicating that R92 is important for the role of OmpC in OM lipid asymmetry. Consistent with this idea, we demonstrated that cells expressing the $OmpC_{R92A}$ variant also exhibit perturbations in OM lipid asymmetry. We further showed that all these *ompC* alleles can rescue severe SDS/EDTA sensitivity known for cells lacking OmpC (Fig. 6*C*), suggesting normal porin function; however, cells expressing

$OmpC_{G19W/R92L}$ and $OmpC_{R92A}$, unlike WT and $OmpC_{R92L}$, are still sensitive to SDS at higher concentrations of EDTA. These phenotypes mirror those observed for cells lacking MlaA, suggesting the loss of Mla function in these mutant strains. It appears that the R92 residue is critical for this function, although it is not clear why the single R92L mutation did not result in SDS/EDTA sensitivity. The exact role of R92 is not known, but the phenotypes observed for the single R92A mutation cannot be due to disruption of OmpC trimerization (Fig. S12). We conclude that OmpC has an active role in maintaining OM lipid symmetry together with MlaA.

Discussion

Osmoporin OmpC interacts with MlaA to maintain lipid asymmetry in the OM; how this complex is organized to extract PLs from the outer leaflet of the OM is not known. In this study, we have employed photoactivatable crosslinking and MD simulations to elucidate the molecular architecture of the OmpC-MlaA complex. We have established that MlaA interacts extensively with OmpC at one of the dimeric interfaces of the porin trimer, and resides entirely within the OM lipid bilayer. In our molecular models, which are consistent with experimental data, MlaA provides a hydrophilic channel that likely allows PL headgroups to translocate across the OM. The overall organization of the OmpC-MlaA complex is quite remarkable, especially how MlaA spans the OM and gains access to outer leaflet PLs. Very few lipoproteins are known to span the OM; some notable examples include the LptDE and Wza translocons, which transports LPS and capsular polysaccharides, respectively. In the LptDE complex, the OM lipoprotein LptE serves as a plug, and stretches across the bilayer through the lumen of the LptD β-barrel (25, 26). In the octameric Wza translocon, each protomer provides a C-terminal α-helix to form a pore that spans the membrane (27). MlaA is unique in that it is essentially an integral membrane protein, capable of forming a channel on its own. In many ways, MlaA behaves like typical OM β-barrel proteins, even though it is predominantly α-helical. Furthermore, being overall a hydrophobic protein also poses a problem for MlaA to transit across the periplasmic space. How MlaA is shielded from the aqueous environment, in addition to the requirement of the Lol system (28), necessitates further investigation.

Our molecular models and functional data on the OmpC-MlaA complex provide a glimpse of how PLs may translocate across the OM during maintenance of lipid asymmetry. One key aspect of MlaA function resides in a hairpin loop structure juxtaposed against the putative hydrophilic channel. Dynamics of this loop appear to control whether MlaA exists in a "closed" or "open" state, and thus access of PLs through the channel. A mutation that likely rigidifies the loop locks MlaA in the non-functional "closed" state (Fig. 5), while mutations that possibly affect interactions with the loop favors the "open" state, and gives rise to gain of function (Fig. 4). Based on detailed study of the OmpC-MlaA models, we speculate that there are two possible routes by which the headgroup of a PL can enter the channel, along with its hydrophobic acyl chains translocating unobstructed through MlaA across the OM (Fig. 7). In the first possible scenario, conformational changes of the hairpin loop (*magenta*) may affect the orientation of the adjacent helix (*blue*), moving it away from OmpC, and allowing PLs specifically bound at the OmpC-MlaA interface (PL_A, as shown in Fig. S8*A*) to gain access into the channel (Fig. 7*A*). Alternatively, movement of the hairpin loop may already provide access into the channel for PLs (PL_B) around the loop region (Fig. 7*B*). Therefore, the hairpin loop may serve as a "lever" to modulate channel access, or as a "lid" that directly gates the channel, respectively. To distinguish between these possibilities, more structural and functional characterization would be required. In particular, high-resolution molecular structures of wild-type and mutant complexes of OmpC-MlaA, with or without PLs bound, would be extremely valuable for defining the route for PL translocation across the OM.

How OmpC participates in maintaining OM lipid asymmetry as part of the complex is not clear, especially given that MlaA alone may provide a channel for PL translocation. It is possible that OmpC may play a passive role, and simply be important for stabilizing the structure of MlaA and ensuring that MlaA is oriented properly in the OM. Consistent with this idea, MlaA underwent the least structural perturbations in the presence of OmpC, as judged by averaged RMSD values during MD simulations (Fig. S6). However, we have previously shown that MlaA also interacts with OmpF, yet removing OmpF has minimal effects on OM lipid asymmetry (12); this argues against a mere passive role for OmpC in PL translocation. Furthermore, we have now identified a specific residue R92 on OmpC that is required for maintaining OM lipid asymmetry (Fig. 6). Therefore, we believe that OmpC plays an active role in the process. R92 lies in

the dimeric interface of the OmpC trimer, which incidentally is where MlaA binds. Even though this residue has been shown to be important for gating the porin (29), it is not obvious how this gating function may influence the translocation of PLs by MlaA. Interestingly, we have observed in coarse-grained MD simulations that outer leaflet PLs tend to concentrate at the dimeric interfaces of the trimer and interact with an extracellular loop ($L4_{OmpC}$), when OmpC is placed in an asymmetric OM model (Fig. S8*C*). In similar simulations of OmpC-MlaA, we also saw a few instances of a PL coming between OmpC and MlaA at the OmpC dimeric interface (Fig. S8*D*). It may be that R92 is somehow important for this phenomenon. In this regard, OmpC may help to engage outer leaflet PLs at the OmpC-MlaA interface so that they can gain access to the putative channel in MlaA for translocation across the OM. This would tie in nicely with one of our proposed mechanisms for how MlaA extracts PLs from the outer leaflet of the OM (Fig. 7*A*). The roles of R92 and $L4_{OmpC}$ in this process should be further characterized.

The OmpC-MlaA complex is proposed to extract PLs from the outer leaflet of the OM and hand them over to MlaC, which resides in the periplasm. Consistent with this idea, *E. coli* MlaC has been crystallized with a bound PL, and shown to interact with a complex of OmpF-MlaA in vitro (14). It is not clear, however, how transfer of PLs from OmpC-MlaA to MlaC takes place, although this must presumably occur in an energy-independent fashion. Since PL movement from the outer to inner leaflets of the OM is entropically disfavored, it is likely that translocation of PLs by the OmpC-MlaA complex would be coupled to transfer to MlaC, i.e. extracted PLs do not go into the inner leaflet. If this were true, it may be possible that MlaC also influences the function of the OmpC-MlaA complex. Specifically, binding of MlaC to the complex may be required for PL extraction from the outer leaflet of the OM. MlaC could alter the structure and/or dynamics of MlaA in the OmpC-MlaA complex, ultimately leading to efficient PL translocation across the OM.

Lipid asymmetry is critical for the OM to function as an effective permeability barrier. Thus, understanding mechanistic aspects of how bacterial cells maintain OM lipid asymmetry would guide us in designing strategies to overcome the barrier. Our work on elucidating the structure and function of the OmpC-MlaA complex has revealed critical insights into the role of a hairpin loop on MlaA in modulating activity, a feature that can be exploited in drug discovery efforts. In particular, small molecules that can

potentially influence dynamics of this loop may induce either loss or gain of function, thereby leading to increased sensitivity to existing antibiotics.

References

1. Kamio Y & Nikaido H (1976) Outer membrane of *Salmonella typhimurium*: accessibility of phospholipid head groups to phospholipase c and cyanogen bromide activated dextran in the external medium. *Biochemistry* 15(12):2561-2570.
2. Funahara Y & Nikaido H (1980) Asymmetric localization of lipopolysaccharides on the outer membrane of *Salmonella typhimurium*. *J Bacteriol* 141(3):1463-1465.
3. Nikaido H (2003) Molecular basis of bacterial outer membrane permeability revisited. *Microbiol Mol Biol Rev* 67(4):593-656.
4. Jia W, *et al.* (2004) Lipid trafficking controls endotoxin acylation in outer membranes of *Escherichia coli*. *J Biol Chem* 279(43):44966-44975.
5. Wu T, *et al.* (2006) Identification of a protein complex that assembles lipopolysaccharide in the outer membrane of *Escherichia coli*. *Proc Natl Acad Sci U S A* 103(31):11754-11759.
6. Okuda S, Sherman DJ, Silhavy TJ, Ruiz N, & Kahne D (2016) Lipopolysaccharide transport and assembly at the outer membrane: the PEZ model. *Nat Rev Microbiol* 14(6):337-345.
7. Shrivastava R, Jiang X, & Chng SS (2017) Outer membrane lipid homeostasis via retrograde phospholipid transport in *Escherichia coli*. *Mol Microbiol* (in press).
8. Dekker N (2000) Outer-membrane phospholipase A: known structure, unknown biological function. *Mol Microbiol* 35(4):711-717.
9. Bishop RE (2005) The lipid A palmitoyltransferase PagP: molecular mechanisms and role in bacterial pathogenesis. *Mol Microbiol* 57(4):900-912.
10. Dalebroux ZD, Matamouros S, Whittington D, Bishop RE, & Miller SI (2014) PhoPQ regulates acidic glycerophospholipid content of the *Salmonella Typhimurium* outer membrane. *Proc Natl Acad Sci U S A* 111(5):1963-1968.

11. Malinverni JC & Silhavy TJ (2009) An ABC transport system that maintains lipid asymmetry in the gram-negative outer membrane. *Proc Natl Acad Sci U S A* 106(19):8009-8014.

12. Chong ZS, Woo WF, & Chng SS (2015) Osmoporin OmpC forms a complex with MlaA to maintain outer membrane lipid asymmetry in *Escherichia coli*. *Mol Microbiol* 98(6):1133-1146.

13. Huang YM, *et al.* (2016) Molecular dynamic study of MlaC protein in Gram-negative bacteria: conformational flexibility, solvent effect and protein-phospholipid binding. *Protein Sci* 25(8):1430-1437.

14. Ekiert DC, *et al.* (2017) Architectures of lipid transport systems for the bacterial outer membrane. *Cell* 169(2):273-285 e217.

15. Thong S, *et al.* (2016) Defining key roles for auxiliary proteins in an ABC transporter that maintains bacterial outer membrane lipid asymmetry. *eLife* 5:e19042.

16. Pages JM, James CE, & Winterhalter M (2008) The porin and the permeating antibiotic: a selective diffusion barrier in Gram-negative bacteria. *Nat Rev Microbiol* 6(12):893-903.

17. Ovchinnikov S, *et al.* (2017) Protein structure determination using metagenome sequence data. *Science* 355(6322):294-298.

18. Basle A, Rummel G, Storici P, Rosenbusch JP, & Schirmer T (2006) Crystal structure of osmoporin OmpC from *E. coli* at 2.0 A. *J Mol Biol* 362(5):933-942.

19. Chin JW, Martin AB, King DS, Wang L, & Schultz PG (2002) Addition of a photocrosslinking amino acid to the genetic code of *Escherichia coli*. *Proc Natl Acad Sci U S A* 99(17):11020-11024.

20. Nakamura K & Mizushima S (1976) Effects of heating in dodecyl sulfate solution on the conformation and electrophoretic mobility of isolated major outer membrane proteins from *Escherichia coli* K-12. *J Biochem* 80(6):1411-1422.

21. Tamm LK, Hong H, & Liang B (2004) Folding and assembly of beta-barrel membrane proteins. *Biochim Biophys Acta* 1666(1-2):250-263.

22. Kozakov D, *et al.* (2017) The ClusPro web server for protein-protein docking. *Nat Protoc* 12(2):255-278.

23. Sutterlin HA, *et al.* (2016) Disruption of lipid homeostasis in the Gram-negative cell envelope activates a novel cell death pathway. *Proc Natl Acad Sci U S A* 113(11):E1565-1574.

24. Naveed H, *et al.* (2012) Engineered oligomerization state of OmpF protein through computational design decouples oligomer dissociation from unfolding. *J Mol Biol* 419(1-2):89-101.

25. Dong H, *et al.* (2014) Structural basis for outer membrane lipopolysaccharide insertion. *Nature* 511(7507):52-56.

26. Qiao S, Luo Q, Zhao Y, Zhang XC, & Huang Y (2014) Structural basis for lipopolysaccharide insertion in the bacterial outer membrane. *Nature* 511(7507):108-111.

27. Dong C, *et al.* (2006) Wza the translocon for *E. coli* capsular polysaccharides defines a new class of membrane protein. *Nature* 444(7116):226-229.

28. Okuda S & Tokuda H (2011) Lipoprotein sorting in bacteria. *Annu Rev Microbiol* 65:239-259.

29. Liu N & Delcour AH (1998) The spontaneous gating activity of OmpC porin is affected by mutations of a putative hydrogen bond network or of a salt bridge between the L3 loop and the barrel. *Protein Eng* 11(9):797-802.

Acknowledgements. We thank Swaine Chen and Varnica Khetrapal (Genome Institute of Singapore, A*STAR) for providing α-OmpC antibody, and reagents for negative selection and assistance in this technique. We also thank Michael Berne (Analytical Core Facility, Tufts Medical School) and Ross Tomaino (Taplin Mass Spectrometry Facility, Harvard Medical School) for performing Edman sequencing and MS/MS, respectively. We gratefully acknowledge computing resources provided by the National Supercomputing Center Singapore (http://www.nscc.sg). Finally, we thank Swaine Chen for critical discussions and comments on the manuscript. J.Y. was supported by the National University of Singapore Graduate School for Integrative Sciences and Engineering scholarship. J.K.M. and P.J.B. acknowledge support from the Singapore Ministry of Education Academic Research Fund Tier 3 grant (MOE2012-T3-1-008). All experimental work was supported by the National University of Singapore Start-up funding, the Singapore Ministry of Education Academic Research Fund Tier 1 and Tier 2 (MOE2013-T2-1-148) grants (to S.-S.C.).

Figure legends

Figure 1. MlaA binds at the dimeric interfaces of the OmpC trimer in vivo. (*A*, *B*) Representative immunoblots showing UV-dependent formation of crosslinks between OmpC and MlaA in Δ*ompC* cells expressing OmpC substituted with *p*Bpa at indicated positions, selected in a (*A*) global, or (*B*) localized search. (*C*) Side (*left*) and top (*right*) views of cartoon representations of the crystal structure of *E. coli* OmpC (PDB ID: 2J1N) (18) with positions that crosslink to MlaA highlighted. Residues selected in the global search for MlaA interaction are colored *cyan* (no crosslinks) and *blue* (sticks; crosslinks detected), while those selected in the localized search are colored *light pink* (no crosslinks) and *red* (sticks; crosslinks detected). The OM boundary is indicated as gray dashed lines. MlaA binding sites are indicated as solid or dashed curves on the top-view representation.

Figure 2. OmpC contacts two specific regions on MlaA. (*A*) SEC profiles and SDS-PAGE analyses of purified OmpC-MlaA-His complex before (*black*) or after (*red*) treatment with trypsin. Peak fractions from SEC were subjected to denaturing SDS-PAGE (15% Tris.HCl gel), followed by Coomassie Blue (CB) staining (*right*). Non-trypsin treated samples were also analysed by seminative SDS-PAGE (*left*). Edman degradation and tandem MS analyses revealed that the MlaA peptide that remains bound to OmpC following trypsin treatment begins at D61 (Fig. S3). (*B*) SDS-PAGE (15% Tris.HCl gel) and immunoblot analyses of purified $OmpC_{pBpa}$-MlaA-His complexes following sequential UV irradiation and trypsin digestion. The resulting $OmpC_{pBpa}$-$MlaA_{peptide}$ crosslinked products were N-terminally sequenced (see Fig. S3). (*C*) Amino acid sequence of MlaA with the two peptides found crosslinked to $OmpC_{pBpa}$ highlighted (*red*: $MlaA_{D61\text{-}K124}$, *blue*: $MlaA_{F133\text{-}R205}$). The signal sequence and α-MlaA binding epitope are underlined and annotated. (*D*) Cartoon representations of the crystal structure of *E. coli* OmpC with positions that crosslink to specific MlaA peptides indicated (*left*), and a structural model of MlaA (17) with peptides crosslinked by $OmpC_{pBpa}$ highlighted (*right*). The OM boundary is indicated as gray dashed lines.

Figure 3. Molecular models of the OmpC-MlaA complex depict how MlaA interacts with OmpC in the OM bilayer. (*A*) A representative OmpC-MlaA structure selected from one of four major clusters in three all-

atomistic MD simulation trajectories. $MlaA_{D61-K124}$ and $MlaA_{F133-R205}$ peptides are highlighted in *red* and *blue*, respectively, as in Fig. 2*D*. The OM boundaries are indicated as gray dashed lines. (*B*) Immunoblots showing UV-dependent formation of a crosslink between MlaA and OmpC in Δ*mlaA* cells expressing $MlaA_{L109pBpa}$-His. As expected, the crosslinked product also exhibits heat-modifiable gel shift, indicative of the presence of OmpC. (*C*) Cartoon representation of OmpC-MlaA expanded from the indicated model in (*A*) with L109 on MlaA highlighted (in sticks).

Figure 4. A triple charge-inversion mutation in a putative hydrophilic channel within MlaA results in gain-of-function phenotypes. (*A*) A representative OmpC-MlaA structure from all-atomistic MD simulations (as in Fig. 3*A*) with its putative channel depicted in *gray*. (*B*) Cartoon representation of MlaA expanded from the indicated model in (*A*) with negatively charged positions mutated to arginine highlighted (in sticks). (*C*) Analysis of SDS/EDTA sensitivity of wild-type (WT) and Δ*mlaA* strains producing indicated MlaA variants at low levels from the pET23/42 vector (p) (12). Serial dilutions of respective cultures were spotted on LB agar plates containing Amp, supplemented with or without 0.50% SDS and 0.5/0.8 mM EDTA, as indicated, and incubated overnight at 37 °C. (*D*) Representative thin layer chromatography (TLC)/autoradiographic analysis of [^{32}P]-labeled lipid A extracted from exponential phase cultures of strains described in (*C*). As a positive control for lipid A palmitoylation, WT cells were treated with 25 mM EDTA for 10 min prior to extraction. Equal amounts of radioactive material were spotted for each sample. Average percentages of palmitoylation of lipid A and the standard deviations were quantified from triplicate experiments and plotted below. Student's t-tests: *, $p < 0.005$ compared to WT with empty vector; **, $p < 0.001$ compared to WT p-*mlaA-His*.

Figure 5. Flexibility in a hairpin loop structure on MlaA distal to the OmpC-MlaA interface is critical for MlaA function. (*A*) Cartoon representation of an OmpC-MlaA model illustrating the region around a hairpin loop on MlaA that is important for function. In the expanded representation, the *3D3R* and *mlaA** mutations, the hairpin loop, and the glycine rich region N-terminal to the loop are colored in *cyan*, *orange* and *black*, respectively. Residues on the hairpin loop chosen for mutation are represented in sticks. (*B*) Analysis of

SDS/EDTA sensitivity of wild-type (WT) and Δ*mlaA* strains producing indicated MlaA loop variants from the pET23/42 vector (p). (*C*) Representative TLC/autoradiographic analysis of [^{32}P]-labeled lipid A extracted from exponential phase cultures of strains described in (*B*). Equal amounts of radioactive material were spotted for each sample. Average percentages of palmitoylation of lipid A and the standard deviations were quantified from triplicate experiments and plotted on the right. Student's t-tests: *, $p < 0.0005$ compared to WT with empty vector. (*D*) Analysis of SDS/EDTA sensitivity of wild-type (WT) and Δ*mlaA* strains producing indicated MlaA variants from the pET23/42 vector (p).

Figure 6. A specific mutation in the dimeric interface of the OmpC trimer results in perturbation in OM lipid asymmetry. (*A*) Cartoon representation of the crystal structure of OmpC trimer illustrating the positions of G19 and R92 region. (*B*) Analysis of SDS/EDTA sensitivity of wild-type (WT) and Δ*ompC* strains producing indicated OmpC variants from the chromosomal locus. (*C*) Representative TLC/autoradiographic analysis of [^{32}P]-labeled lipid A extracted from stationary phase cultures of strains described in (*B*). Equal amounts of radioactive material were spotted for each sample. Average percentages of palmitoylation of lipid A and the standard deviations were quantified from triplicate experiments and plotted on the right. Student's t-tests: *, $p < 0.005$ compared to Δ*ompC*::*ompC*.

Figure 7. Possible routes for outer leaflet PL access into the putative channel of MlaA in the OmpC-MlaA complex. In possibility (*A*), the flexible hairpin loop (*magenta*) may move away from the core structure of MlaA (*green*) while pulling along the adjacent α-helix (*blue*), thus exposing the hydrophilic channel (*red*) to the PL (PL_A, *yellow*) that is found at the OmpC-MlaA interface. In possibility (*B*), the hydrophilic channel is accessible as the result of the movement of the hairpin loop alone, allowing PLs (PL_B, *yellow*) to enter from the side of MlaA. In both (*A*) and (*B*), the hydrophobic acyl chains of the PL entering the channel would be able to cross the OM unobstructed via MlaA. Top (*top panels*) and side views (*bottom panels*) of the OmpC-MlaA model are shown. The OM boundary is indicated as gray dashed lines.

Figure 1

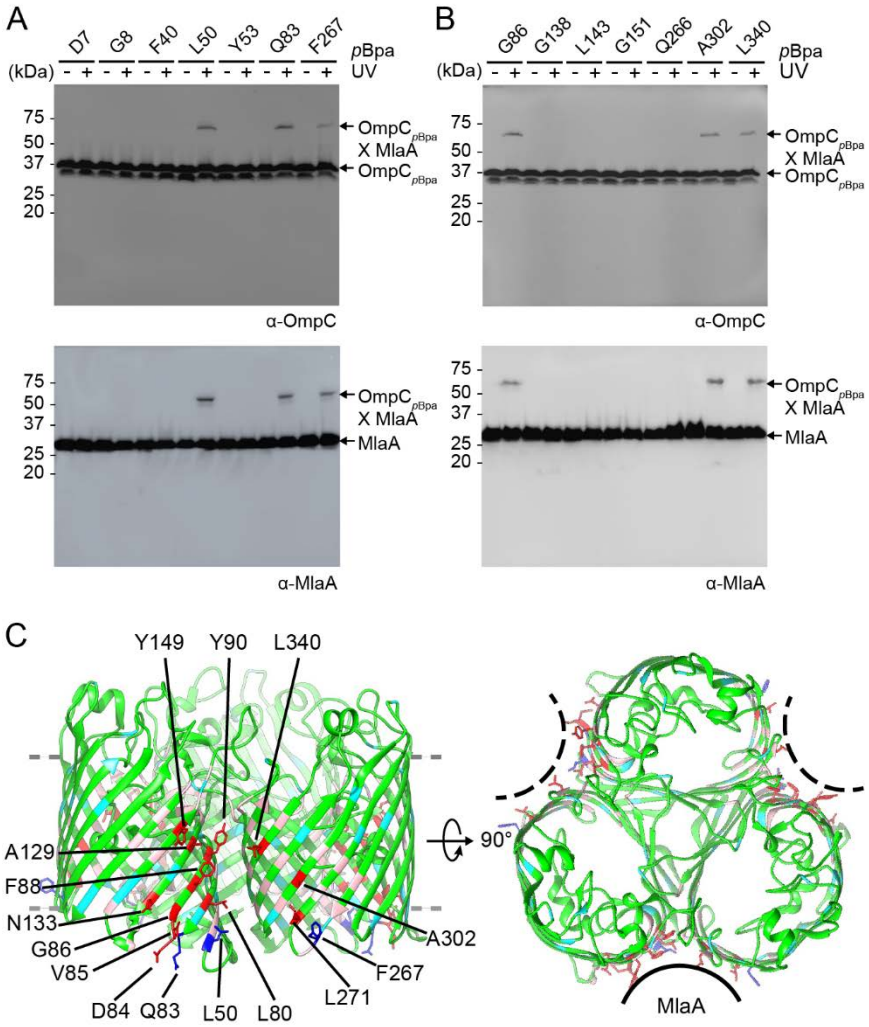
A
D7
G8
F40
L50
Y53
Q83
F267
pBpa
(kDa)
UV
75
50
37
25
20
OmpC pBpa
X MlaA
OmpC pBpa
α-OmpC
MlaA
α-MlaA
B
G86
G138
L143
G151
Q266
A302
L340
C
Y149
Y90
L340
A129
F88
N133
G86
V85
D84
Q83
L50
L80
L271
F267
A302
90°
MlaA

Figure 2

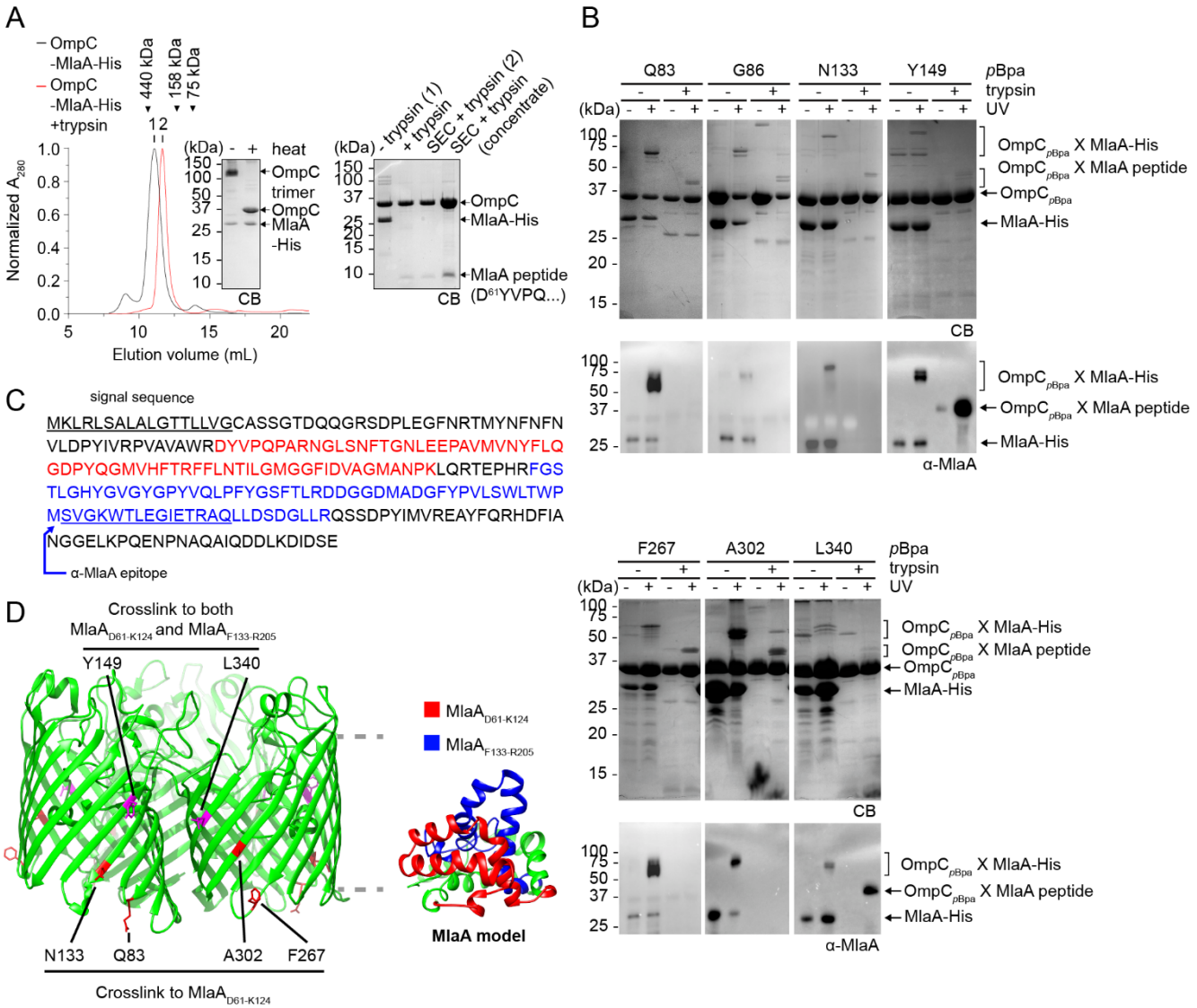
A
OmpC -MlaA-His
OmpC -MlaA-His +trypsin
440 kDa
158 kDa
75 kDa
Normalized A_{280}
Elution volume (mL)
(kDa) - + heat
OmpC trimer
OmpC
MlaA -His
CB
(kDa) - trypsin (1) + trypsin SEC + trypsin (2) SEC + trypsin (concentrate)
OmpC
MlaA-His
MlaA peptide (D61YVPQ...)
B
Q83 G86 N133 Y149
pBpa
trypsin
UV
OmpC$_{pBpa}$ X MlaA-His
OmpC$_{pBpa}$ X MlaA peptide
OmpC$_{pBpa}$
MlaA-His
α-MlaA
F267 A302 L340
C
signal sequence
MKLRLSALALGTTLLVGCASSGTDQQGRSDPLEGFNRTMYNFNFN
VLDPYIVRPVAVAWRDYVPQPARNGLSNFTGNLEEPAVMVNYFLQ
GDPYQGMVHFTRFFLNTILGMGGFIDVAGMANPKLQRTEPHRFGS
TLGHYGVGYGPYVQLPFYGSFTLRDDGGDMADGFYPVLSWLTWP
MSVGKWTLEGIETRAQLLDSDGLLRQSSDPYIMVREAYFQRHDFIA
NGGELKPQENPNAQAIQDDLKDIDSE
α-MlaA epitope
D
Crosslink to both MlaA$_{D61-K124}$ and MlaA$_{F133-R205}$
Y149
L340
N133
Q83
A302
F267
Crosslink to MlaA$_{D61-K124}$
MlaA$_{D61-K124}$
MlaA$_{F133-R205}$
MlaA model

Figure 3

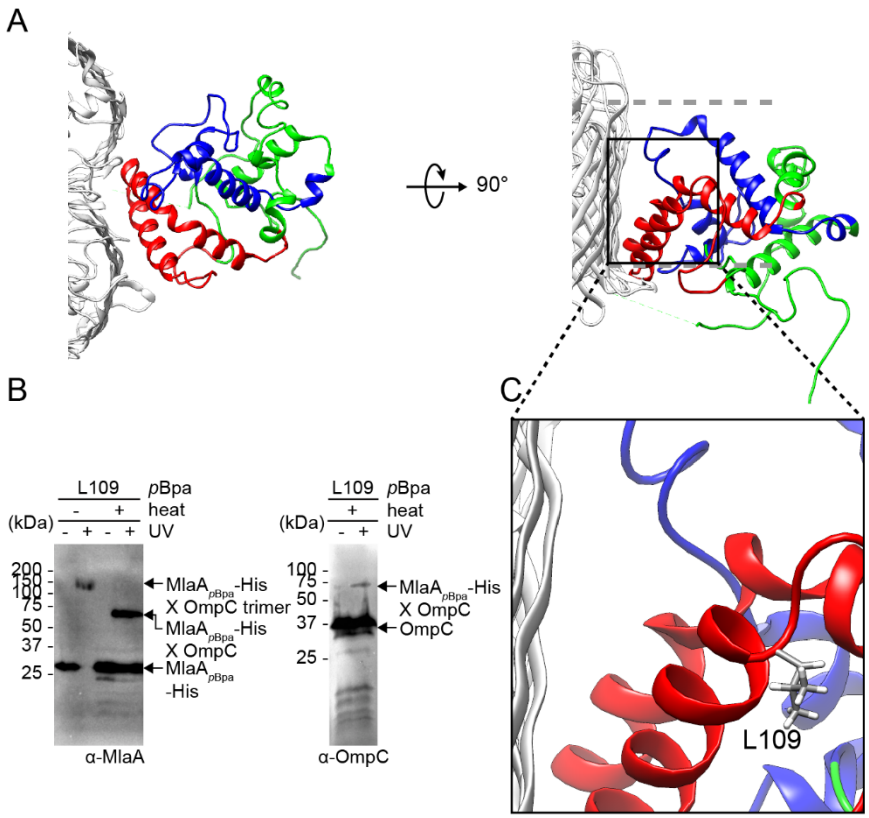
A
90°
B
C
L109
pBpa
heat
UV
(kDa)
200
150
100
75
50
37
25
MlaA$_{pBpa}$-His X OmpC trimer
MlaA$_{pBpa}$-His X OmpC
MlaA$_{pBpa}$-His
α-MlaA
MlaA$_{pBpa}$-His X OmpC
OmpC
α-OmpC
L109

Figure 4

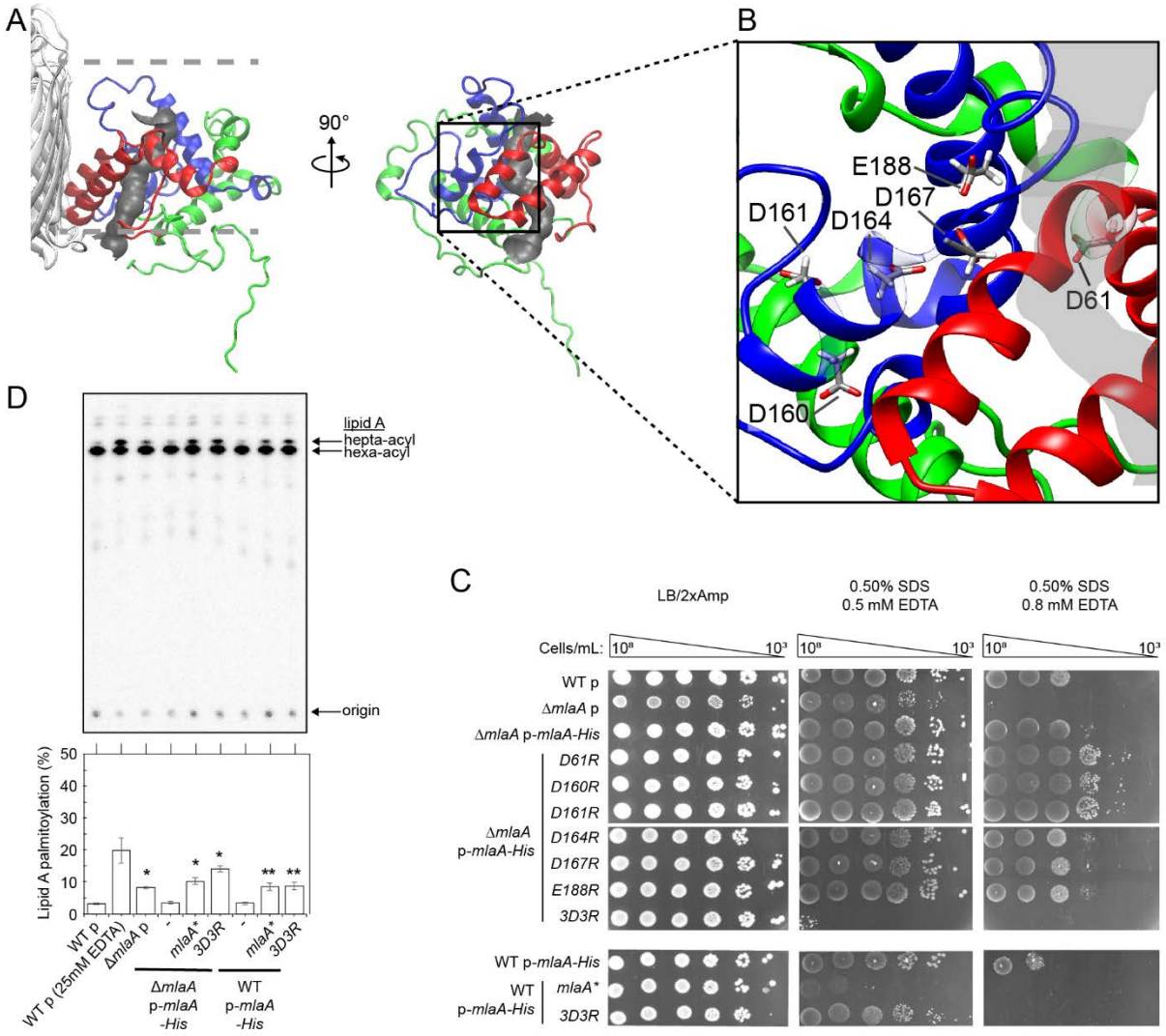
A
90°
B
E188
D167
D161
D164
D61
D160
D
lipid A
hepta-acyl
hexa-acyl
origin
Lipid A palmitoylation (%)
50
40
30
20
10
0
WT p
WT p (25mM EDTA)
ΔmlaA p
-
mlaA*
3D3R
-
mlaA*
3D3R
ΔmlaA p-mlaA -His
WT p-mlaA -His
C
LB/2xAmp
0.50% SDS 0.5 mM EDTA
0.50% SDS 0.8 mM EDTA
Cells/mL:
10⁸
10³
WT p
ΔmlaA p
ΔmlaA p-mlaA-His
D61R
D160R
D161R
D164R
D167R
E188R
3D3R
ΔmlaA p-mlaA-His
WT p-mlaA-His
mlaA*
3D3R
WT p-mlaA-His

Figure 5

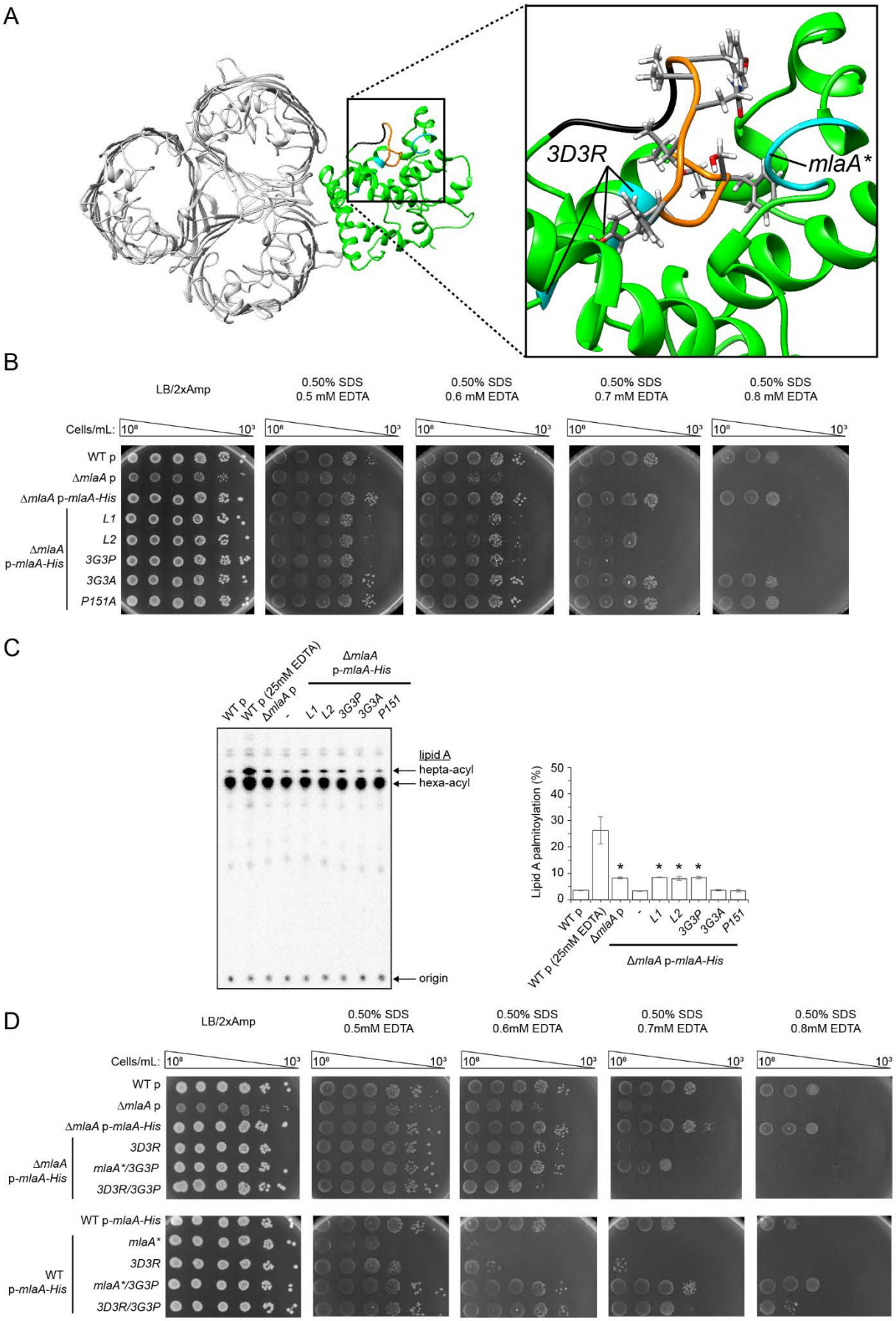
A
3D3R
mlaA*
B
LB/2xAmp
0.50% SDS 0.5 mM EDTA
0.50% SDS 0.6 mM EDTA
0.50% SDS 0.7 mM EDTA
0.50% SDS 0.8 mM EDTA
Cells/mL: 10⁸ 10³
WT p
ΔmlaA p
ΔmlaA p-mlaA-His
ΔmlaA p-mlaA-His
L1
L2
3G3P
3G3A
P151A
C
WT p
WT p (25mM EDTA)
ΔmlaA p
ΔmlaA p-mlaA-His
L1 L2 3G3P 3G3A P151
lipid A
hepta-acyl
hexa-acyl
origin
Lipid A palmitoylation (%)
50
40
30
20
10
0
ΔmlaA p-mlaA-His
D
LB/2xAmp
0.50% SDS 0.5mM EDTA
0.50% SDS 0.6mM EDTA
0.50% SDS 0.7mM EDTA
0.50% SDS 0.8mM EDTA
Cells/mL: 10⁸ 10³
WT p
ΔmlaA p
ΔmlaA p-mlaA-His
3D3R
mlaA*/3G3P
3D3R/3G3P
WT p-mlaA-His
mlaA*
3D3R
mlaA*/3G3P
3D3R/3G3P

Figure 6

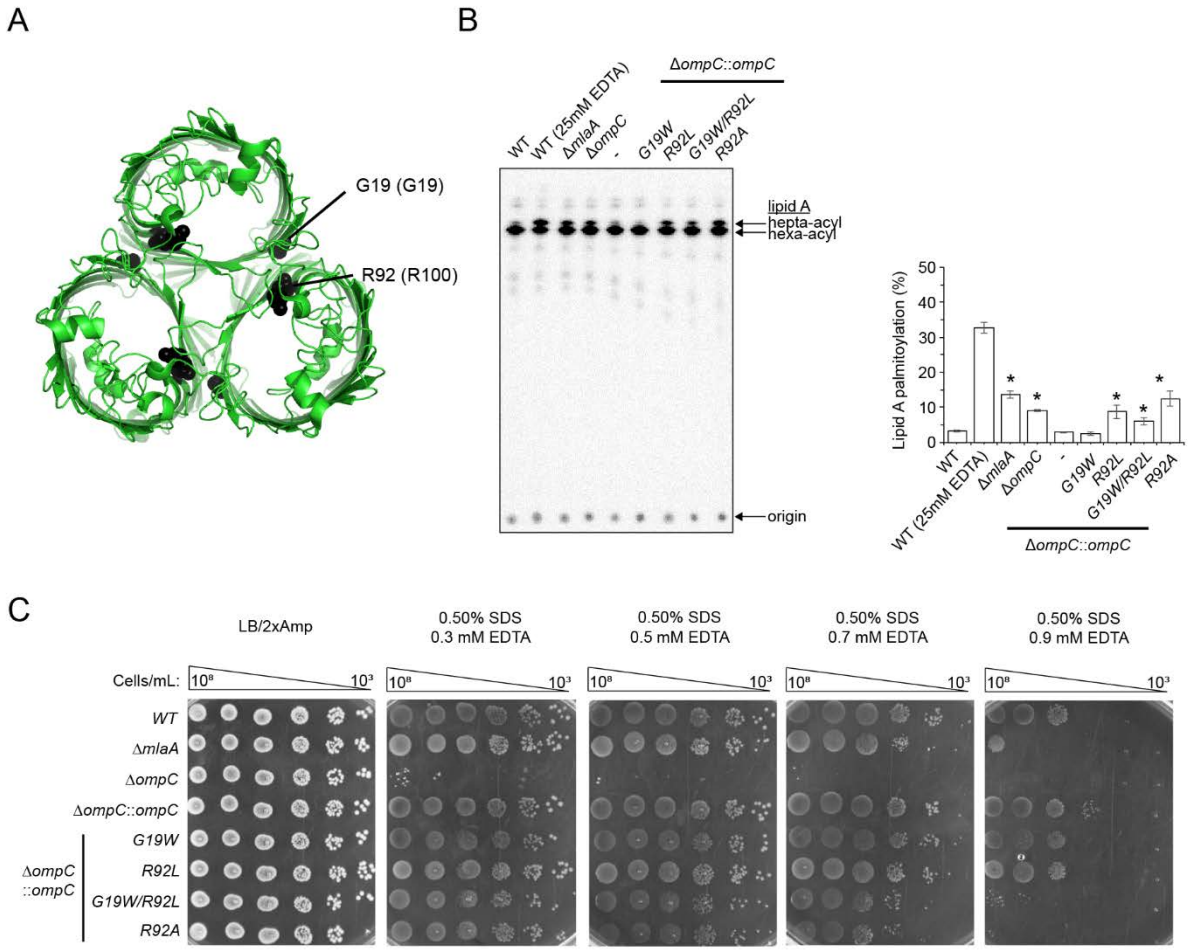
A
G19 (G19)
R92 (R100)
B
ΔompC::ompC
WT
WT (25mM EDTA)
ΔmlaA
ΔompC
-
G19W
R92L
G19W/R92L
R92A
lipid A
hepta-acyl
hexa-acyl
origin
Lipid A palmitoylation (%)
50
40
30
20
10
0
C
LB/2xAmp
0.50% SDS
0.3 mM EDTA
0.50% SDS
0.5 mM EDTA
0.50% SDS
0.7 mM EDTA
0.50% SDS
0.9 mM EDTA
Cells/mL:
10⁸
10³
WT
ΔmlaA
ΔompC
ΔompC::ompC
G19W
R92L
G19W/R92L
R92A
ΔompC
::ompC

Figure 7

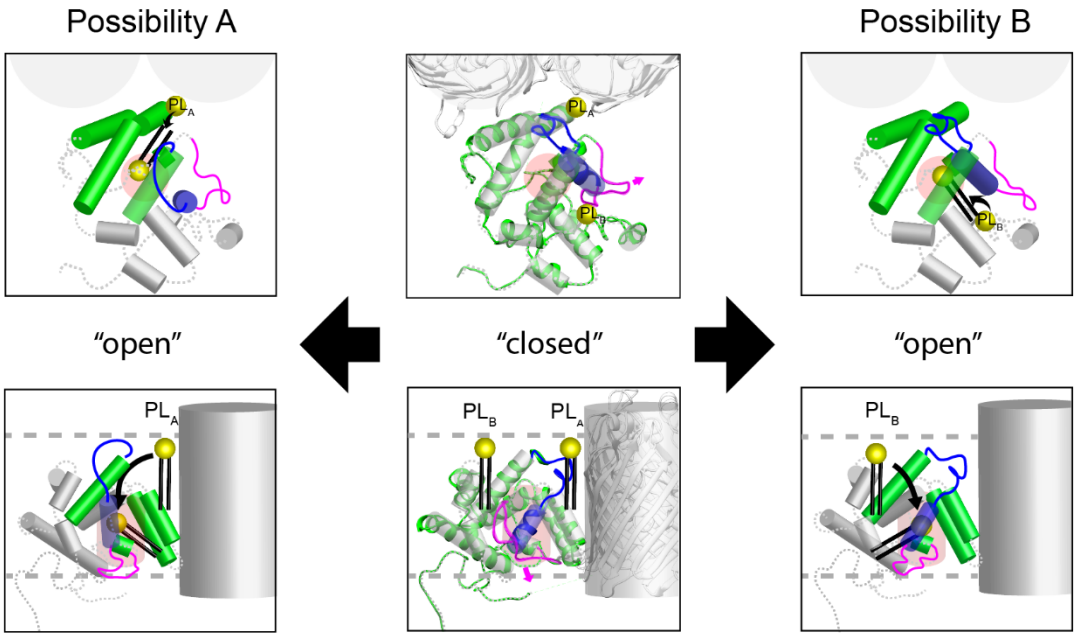
Possibility A
Possibility B
PL_A
PL_B
"open"
"closed"
"open"
PL_A
PL_B
PL_A
PL_B